Robust, self-adhesive, reinforced polymeric nanofilms enabling gas-permeable dry electrodes for long-term application

Yan Wang[a], Sunghoon Lee[a], Haoyang Wang[a], Zhi Jiang[a], Yasutoshi Jimbo[a], Chunya Wang[a], Binghao Wang[a], Jae Joon Kim[a], Mari Koizumi[a], Tomoyuki Yokota[a], and Takao Someya[a,1]

[a]Department of Electrical Engineering and Information Systems, The University of Tokyo, Tokyo 113-8656, Japan

Edited by John A. Rogers, Northwestern University, Evanston, IL, and approved August 4, 2021 (received for review June 28, 2021)

Robust polymeric nanofilms can be used to construct gas-permeable soft electronics that can directly adhere to soft biological tissue for continuous, long-term biosignal monitoring. However, it is challenging to fabricate gas-permeable dry electrodes that can self-adhere to the human skin and retain their functionality for long-term (>1 d) health monitoring. We have succeeded in developing an extraordinarily robust, self-adhesive, gas-permeable nanofilm with a thickness of only 95 nm. It exhibits an extremely high skin adhesion energy per unit area of 159 μJ/cm^2. The nanofilm can self-adhere to the human skin by van der Waals forces alone, for 1 wk, without any adhesive materials or tapes. The nanofilm is ultradurable, and it can support liquids that are 79,000 times heavier than its own weight with a tensile stress of 7.82 MPa. The advantageous features of its thinness, self-adhesiveness, and robustness enable a gas-permeable dry electrode comprising of a nanofilm and an Au layer, resulting in a continuous monitoring of electrocardiogram signals with a high signal-to-noise ratio (34 dB) for 1 wk.

dry electrodes | adhesive nanofilms | gas-permeable sensors | long-term health monitoring

Polymeric films of nanoscale thickness are important building blocks of soft electronics that can directly adhere to soft biological tissue for medical diagnostics, therapeutics, health monitoring, and human–machine interactions (1–3). Such fabricated soft electronics enable mechanical compatibility with the living body (4). This capability is in great demand in skin electronics for high-fidelity health monitoring (5, 6). Meanwhile, to realize long-term monitoring, skin sensors should survive continuous attachment to the skin without external fixturing and/or adhesives (7–9). Currently, the recorded biosignals using existing wet medical electrodes deteriorate over long-term attachment, owing to issues such as skin irritation and dehydration (10). This limitation underscores the need to develop dry electrodes that can remain functional during prolonged wearing (11).

For practical implementation of long-term use, dry electrodes must be stretchable, gas permeable, and have robust bonding to the human skin during daily living. Because bulky, thick devices have inferior skin compliance, encouraging progress has been made to reduce the thickness of polymeric substrates (12–14). For example, an ∼3-μm-thick poly(methyl methacrylate) (PMMA)/polyimide) film was integrated with an Au layer to achieve an electrocardiogram (ECG) electrode. The device could be stretched to 30% strain and sustain 48 h wearing (15). By decreasing the thickness to a few hundred nanometers, dry electrodes exhibit self-adhesiveness to the human skin without external fixturing and/or adhesives. External fixturing and/or adhesives should be avoided due to their bulky format. For example, a 460-nm- thick linear graphene/PMMA electrode can be stretched to ∼20% strain and adhere to the human skin for several hours (16). Furthermore, gas permeability can be achieved using thinner nanofilms or nanomesh structures (17, 18). A 160-nm-thick breathable electrode was developed using a styrene–ethylene/butylene–styrene (SEBS) nanofilm and silver nanowires (19). The dry electrodes could survive 5 h wearing without causing any discomfort to the subject.

However, it is challenging to fabricate a robust, gas-permeable dry electrode that can self-adhere to the human skin and remain its functionality for long-term (>1 d) health monitoring (*SI Appendix*, Table S1) (19–27). The main reason for this is the canonical trade-off between mechanical robustness and geometry thinness. Polymeric films of nanometer-scale thickness easily fracture because of the restraining mechanical robustness. Therefore, it is difficult to integrate electrical materials with such thin, fragile nanofilms to fabricate active sensors. This mechanical limitation also makes such electrodes unable to withstand stretching to more than 30% strain for on-skin applications (28, 29). Furthermore, the improvement of mechanical durability usually leads to thick devices with inadequate gas permeability, which cause skin inflammation or other health concerns when worn over long periods (20, 21).

Herein, we report an extraordinarily robust, self-adhesive, gas-permeable nanofilm with a thickness of only 95 nm. It exhibits extremely high skin adhesion energy per unit area of 159 μJ/cm^2 in which a nanofilm adheres to the human skin by van der Waals forces alone, without any adhesive materials or tapes, for 1 wk. Furthermore, the nanofilm exhibits excellent durability. It can support liquids that are 79,000 times heavier than its own weight with a tensile stress of 7.82 MPa. Owing to its thinness, self-adhesiveness, and robustness, a gas-permeable dry electrode made of gold on a nanofilm allows continuous monitoring of ECG signals with a high signal-to-noise ratio (34 dB) for 1 wk.

Significance

We have succeeded in fabricating a highly robust, adhesive, gas-permeable free-standing polymeric nanofilm with a thickness of less than 100 nm. A gas-permeable dry electrode comprising of a nanofilm and an Au layer can adhere to the human skin by van der Waals forces alone for 1 wk for high-fidelity electrocardiogram recording. Our method has overcome the major bottleneck in continuously monitoring biosignals for a long period of time with high precision under daily life conditions, opening up new opportunities in a wide range of applications in fields such as medicine, healthcare, sports, fitness, virtual reality, and entertainment.

Author contributions: Y.W. and S.L. designed research; Y.W. performed research; Y.W., S.L., H.W., Z.J., Y.J., C.W., B.W., J.J.K., M.K., T.Y., and T.S. analyzed data; and Y.W. and T.S. wrote the paper.

The authors declare no competing interest.

This article is a PNAS Direct Submission.

[1]To whom correspondence may be addressed. Email: someya@ee.t.u-tokyo.ac.jp.

This article contains supporting information online at https://www.pnas.org/lookup/suppl/doi:10.1073/pnas.2111904118/-/DCSupplemental.

Published September 13, 2021.

Results

Fabrication and Characterizations of Free-Standing Polyurethane–PDMS Nanofilm. To overcome the typical trade-off between mechanical robustness and geometry thinness in polymeric nanofilms, we developed polyurethane nanofiber–reinforced polydimethylsiloxane (PDMS) nanofilms. Fig. 1*A* shows a freely suspended polyurethane–PDMS nanofilm holding large amounts of liquids. We observe the extension of the nanofilm while the liquid beads up (Movie S1 and *SI Appendix*, Fig. S1). Fig. 1*B* shows a cross-sectional scanning electron microscopy (SEM) image of the polyurethane–PDMS nanofilm adhering to an anodisc substrate (*SI Appendix*, Fig. S2). The polyurethane–PDMS nanofilm is strong enough to hold liquids that are 79,000 times heavier than its own weight with an average thickness of only ∼95 nm and a tensile stress of 7.82 MPa (30) (*SI Appendix*, Fig. S1). In contrast, the pure PDMS film breaks when the liquid volume exceeds 3 mL, even with a thickness of ∼720 nm (*SI Appendix*, Figs. S3 and S4). The tensile stress is only 0.53 MPa at a liquid volume of 3 mL.

The fabrication of the free-standing nanofilms involved two steps. First, a polyurethane nanofiber sheet was fabricated by electrospinning. The morphologies of electrospun nanofibers are shown in *SI Appendix*, Fig. S5. Here, the density of the polyurethane nanofiber was 0.36 mg/cm^2. In the second fabrication step, a simple yet efficient dip-coating technique was used to form thin polymeric films on the existing polyurethane nanoweb (Fig. 2 *A*–*C* and Movie S2). The dip-coating solution was prepared from PDMS diluted by hexane. After the solvent evaporated quickly, a pinhole-free film formed with ultrathin PDMS suspended across the polyurethane nanofibers. Fig. 2 *A* and *C* depict the microscopic characterizations of the polyurethane nanofiber sheet and the resulting polyurethane–PDMS nanofilm, respectively. It is noteworthy that the obtained polymeric nanofilm requires no sacrificing layer or solvent-soluble sacrificial substrate, which are commonly employed to fabricate traditional polymeric nanosheets (31).

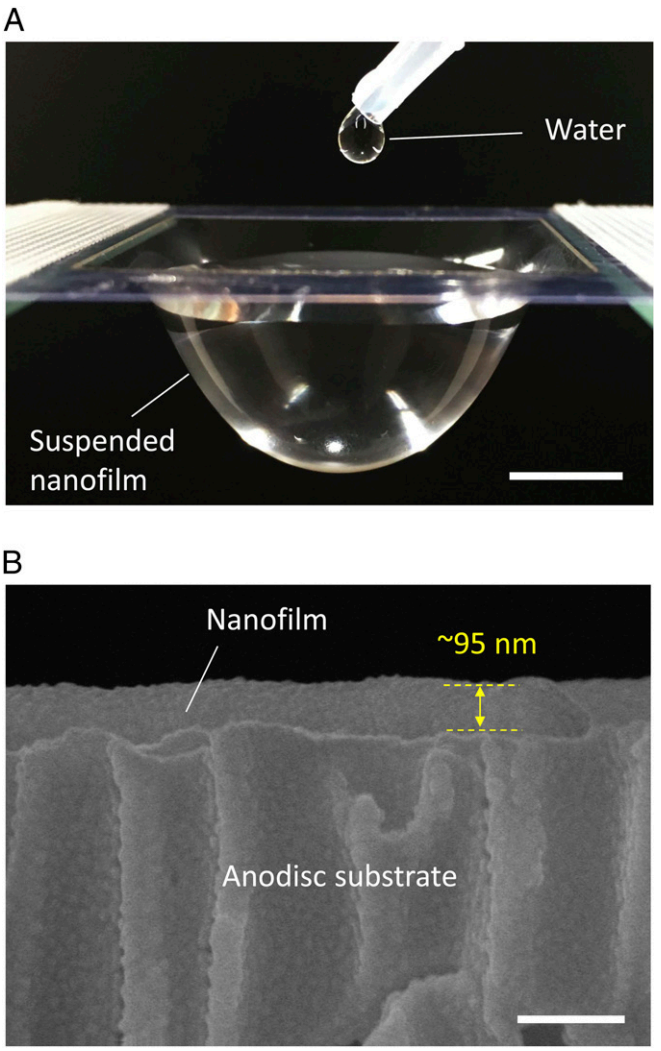

Fig. 1. Robustness and thinness of polyurethane–PDMS nanofilm. (*A*) Photograph of a suspended nanofilm holding liquid (8 g). (Scale bar, 10 mm.) (*B*) Cross-sectional SEM image of the nanofilm attached on anodisc substrate. 70-nm-thick Au was coated onto the cross-section to achieve conductivity. (Scale bar, 200 nm.)

The film-forming process is illustrated in *SI Appendix*, Fig. S6*A*, demonstrating the polyurethane–PDMS nanomesh evolving to the polyurethane–PDMS nanofilm while gradually increasing PDMS concentration in the dip-coating solution. The capability of large-scale fabrication, mechanical flexibility, and high transmittance is demonstrated in Fig. 2*D* and *SI Appendix*, Fig. S6 *B*–*D*. The surface of the nanofilm is not flat because of randomly distributed polyurethane nanofibers (*SI Appendix*, Fig. S6 *E* and *F*). Although the diameter of nanofibers is around 185 nm, the thickness of pure PDMS area is much thinner, with tens of nanometers (*SI Appendix*, Fig. S2). Furthermore, the pure PDMS area has a fraction area of nearly 85%. Therefore, the average thickness is calculated to be 95 nm, in which the nanofibers and their junctions contribute to the higher peaks on the surface profile (*SI Appendix*, Fig. S6*F*). The rough feature may also be caused by solvent evaporation–induced flows on the surface of the liquid layer during the evaporation process. The aspect ratio of length to thickness is greater than 10^6, leading to the uniqueness of interfacial and mechanical properties, such as self-adhesiveness, flexibility, robustness, and gas permeability, which will be explored later in this work. The ∼95-nm-thick polyurethane–PDMS nanofilm is herein referred to as 'nanofilm" unless otherwise specified.

Note that the dip-coating technique can be used as a universal approach to generate free-standing polymeric nanofilms. Here, arbitrary electrospun nanofibers serve as the backbone for scaffolding. A polymer that is soluble in a solvent with high volatility can effectively "fill" the voids of electrospun nanoweb to realize film formation induced by fast solvent evaporation. As a proof of concept, various polymeric nanofilms, such as polyurethane–Ecoflex, polyurethane–polyvinyl alcohol (PVA), PVA–PDMS, and PVA–polyurethane, were fabricated and are shown in *SI Appendix*, Fig. S7.

Flexural rigidity is highly correlated with the conformability of a plate film to a three-dimensional (3D) surface, which is defined as $D = \frac{Et^3}{12(1-\nu^2)}$ (5). Here, E, t, and ν respectively represent Young's modulus, thickness, and Poisson's ratio of the thin film. The cubic dependence on thickness indicates that reducing thickness is the most effective strategy for decreasing flexural rigidity. A comparison of various free-standing polymeric nanofilms ($t < 1$ μm) is shown in *SI Appendix*, Table S2. To achieve a high skin adhesion property, the flexural rigidity of a polymeric film should be less than 10^{-2} nN m, which is within the range of living brain slices (per unit width) (5). The flexural rigidity of the polyurethane–PDMS nanofilm is calculated to be 1.19×10^{-6} nN m, which is lower than that of the 53-nm-thick polyarylate nanofilm (32), 77-nm-thick poly(3,4-ethylenedioxythiophene)/poly(styrenesulfonate) (PEDOT/PSS) nanofilm (33), 560-nm-thick PDMS nanofilm (34), 100-nm-thick aluminosilicate nanotube (ASNT)/PDMS nanofilm (35), 212-nm-thick polystyrene–polybutadiene–polystyrene (SBS) triblock copolymer nanofilm (36), and even the 23-nm-thick poly(-L-lactic acid) (PLLA) nanofilm (37). Although the 8.4-nm-thick polyamide nanofilm (38) and 70-nm-thick PDMS (28) have a flexural rigidity of less than 10^{-7} nN m, they both suffer from limited mechanical robustness and/or stretchability. Moreover, it is challenging

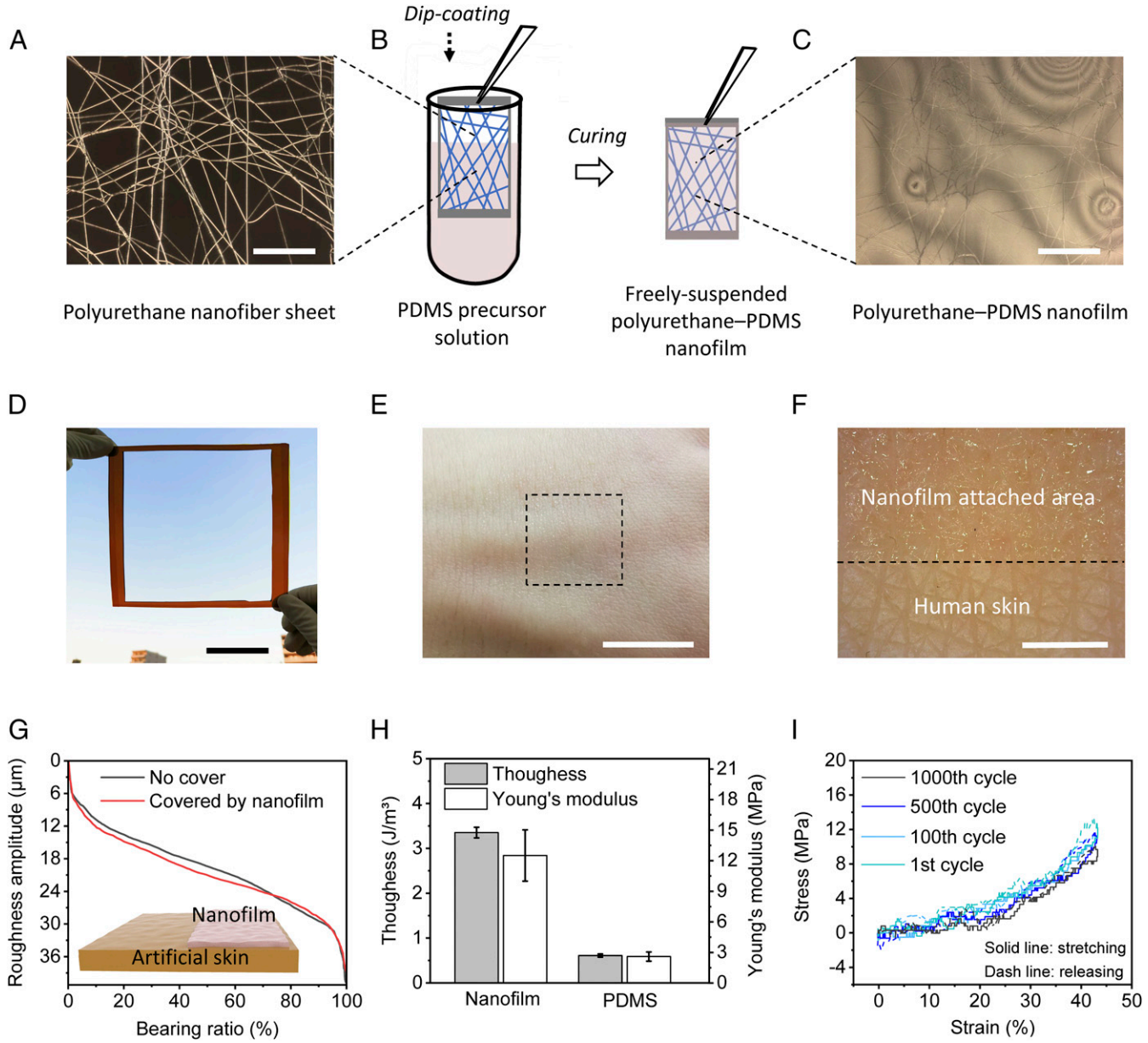

Fig. 2. Fabrication and characterization of free-standing polyurethane–PDMS nanofilms. (*A*) Microscopic image of polyurethane nanofiber sheet. (Scale bar, 20 μm.) (*B*) Schematic fabrication process at room temperature: self-assembly of polymeric nanofilms by dip coating. (*C*) Microscopic image of polyurethane–PDMS nanofilm. (Scale bar, 20 μm.) (*D*) Photograph of a large freely suspended nanofilm. (Scale bar, 5 cm.) (*E*) Close-up photograph of the back of a hand with the nanofilm attached; the dotted rectangle is the area where the nanofilm is attached. (Scale bar, 2 cm.) (*F*) Microscopic image of the edge area of the rectangle in *E*. (Scale bar, 5 mm.) (*G*) Characteristics of the surface texture: Abbott–Firestone curves of the surface of bare artificial skins and nanofilm-covered artificial skins under biaxial stretching to 10% strain. (*H*) Comparisons of toughness and Young's modulus of the nanofilm and pure PDMS film. Error bars represent the SD of the measured values ($n = 3$). (*I*) The 1,000-cycle tensile stress of the nanofilm. Nanofilm thickness: ~95 nm.

to fabricate SEBS nanofilms with sizes larger than 10 cm, owing to the fabrication method of bubble blowing (19).

The nanofilms exhibited high compliance to flat silicon wafers (*SI Appendix*, Fig. S8 *A* and *B*) and porous anodisc substrates (*SI Appendix*, Fig. S8 *C* and *D*). Fig. 2 *E* and *F* show the unperceivable attachment and appearance of the nanofilm on the human skin because of ultralow flexural rigidity and high transparency. To investigate the roughness adaptation to the skin, we attached nanofilms and pure PDMS films onto the artificial skin and scrutinized the roughness features of the surface. The results were quantitatively analyzed using Abbott–Firestone curves, which enabled complementary analysis of surface texture in terms of the roughness height (39). It is demonstrated that the nanofilm-covered artificial skins display surface roughness features that are identical to those of bare artificial skins (*SI Appendix*, Fig. S9*A*). The SEM (*SI Appendix*, Fig. S8 *E* and *F*) and microscopic (*SI Appendix*, Fig. S9 *A* and *B*) observations reveal consistent results in which the peaks and valleys of the curvilinear surface are well preserved on the nanofilm-covered artificial skins. In contrast, the PDMS-covered artificial skin exhibits inferior compliance, owing to its larger thickness and smooth surface (*SI Appendix*, Fig. S9 *C* and *D*). The good conformability of the nanofilm is maintained, even under a biaxially stretched state (Fig. 2*G*). This is attributed to the ability of the nanofilm to stretch and remain in intimate contact with the underlying curvilinear surface (*SI Appendix*, Fig. S9 *E* and *F*).

We then further compared the tensile stress of the nanofilms and pure PDMS films (~20 μm thick). Fig. 2*H* shows that the toughness and Young's modulus of the nanofilms are 3.4 ± 0.1 J/m^3 and 12.5 ± 2.6 MPa, respectively, both of which are approximately five times larger than those of pure PDMS films (40). In addition, the nanofilm exhibits high mechanical durability by 1,000 cycle stretching and releasing to 42% uniaxial strain (Fig. 2*I*).

Then, we changed the density of the polyurethane nanofiber sheet (0.36 to 3.60 mg/cm^2, *SI Appendix*, Fig. S10*A*) and the concentration of the PDMS solution (2.27 to 16.7 weight percentage [wt%]) to fabricate polyurethane–PDMS films with a thickness ranging from 0.095 to 7.654 μm (*SI Appendix*, Fig. S10*B*). The amount of attached PDMS was the key factor affecting the thickness of the suspended films. A higher PDMS concentration led to thicker films, which is observable in the microscopic characterizations (*SI Appendix*, Fig. S10 *C–F*).

Young's Modulus and Toughness of Free-Standing Polyurethane–PDMS Nanofilms. To enhance the mechanical properties like tensile strength, modulus, and toughness of a nanofiber-reinforced composite, a typical approach is to increase the reinforcing effect by increasing the nanofiber content (41, 42). In this work, the ratio between PDMS and nanofiber was determined by varied nanofiber density and film thickness. As shown in Fig. 3 *A* and *B*, the trends of mechanical strength of the polyurethane–PDMS films are the same for both low (0.36 mg/cm^2) and high (3.60 mg/cm^2) polyurethane nanofiber densities, while the thickness increases. With respect to the films with nanofiber density of 0.36 mg/cm^2, the Young's modulus and toughness of the polyurethane–PDMS films with thicknesses of 0.095, 0.213, and 1.653 μm decrease from 12.5 ± 2.3 to 1.1 ± 0.3 MPa and 3.4 ± 0.1 to 0.4 ± 0.02 J/m^3, respectively. For films with nanofiber densities of 3.60 mg/cm^2, the Young's modulus and toughness of the polyurethane–PDMS films with thicknesses of 0.461, 1.239, and 1.925 μm decrease from 30.9 ± 2.1 to 7.8 ± 0.3 MPa and 7.1 ± 0.04 to 3.1 ± 0.2 J/m^3, respectively (Fig. 3 *D* and *E*). In the case of polyurethane–PDMS films with comparable thicknesses (0.213 to 0.255 μm) from varied nanofiber densities, the trend of mechanical strength is the same (Fig. 3*C*). This is because higher area content of polyurethane nanofiber leads to stronger reinforcement effect. For the 0.213- to 0.255-μm-thick polyurethane–PDMS nanofilms with nanofiber densities of 0.36, 1.08, and 2.16 mg/cm^2, the Young's modulus is 5.7 ± 1.1, 23.4 ± 1.9, and 30.2 ± 2.1 MPa, respectively, and the toughness is 2.2 ± 0.1, 4.8 ± 0.2, and 9.1 ± 0.2 J/m^3, respectively

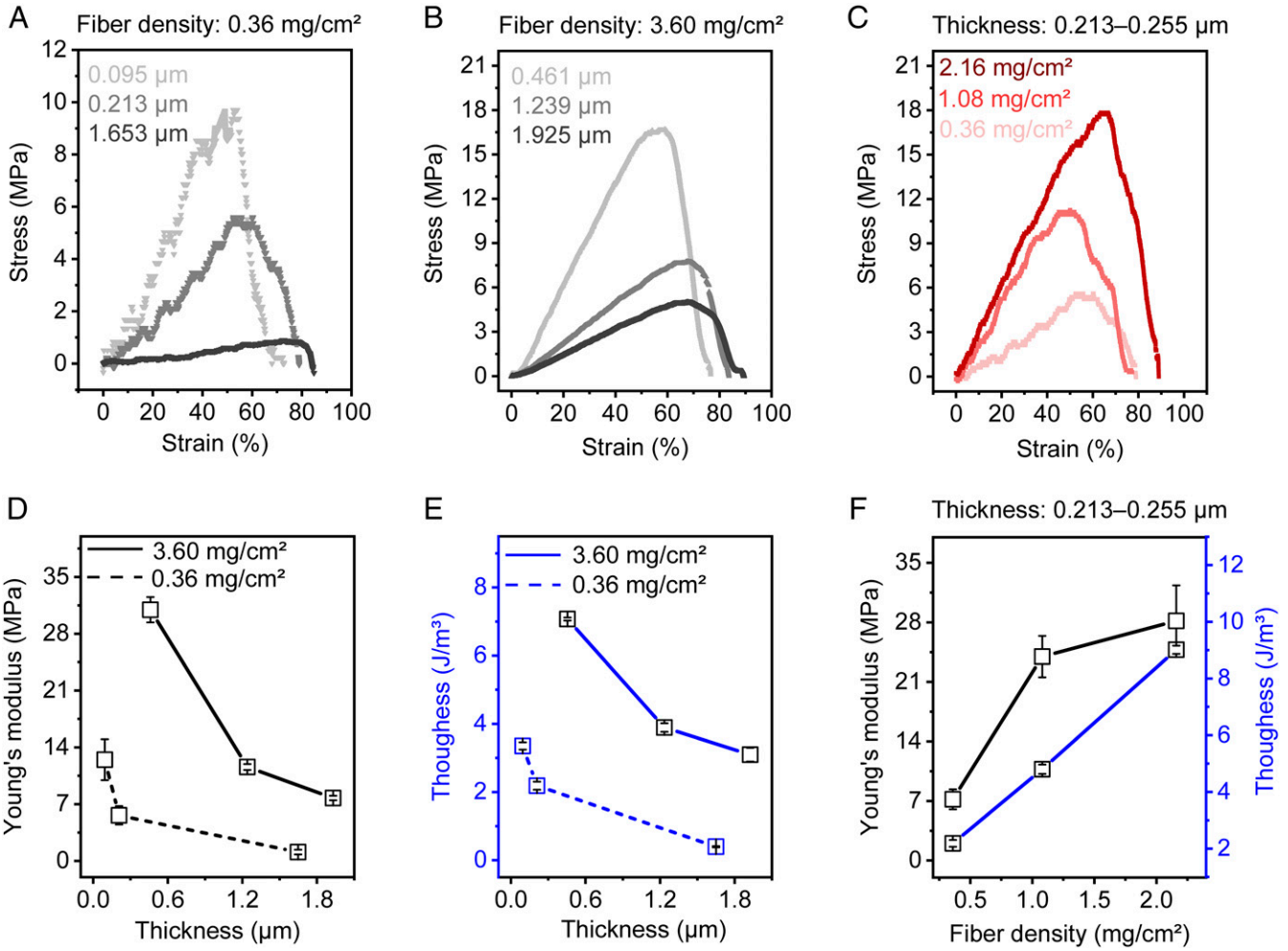

Fig. 3. Young's modulus and toughness of free-standing polyurethane–PDMS films with different nanofiber densities and film thicknesses. (*A*) Tensile stress curves of different polyurethane–PDMS films (0.095, 0.213, and 1.653 μm thick). Fiber density: 0.36 mg/cm^2. (*B*) Tensile stress curves of different polyurethane–PDMS films (0.461, 1.239, and 1.925 μm thick). Fiber density: 3.60 mg/cm^2. (*C*) Tensile stress curves of nanofilms with similar thicknesses (0.213 to 0.255 μm) from different polyurethane nanofibers. Fiber densities: 0.36, 1.08, and 2.16 mg/cm^2. (*D*) Comparisons of Young's modulus for polyurethane–PDMS films from *A* and *B*. (*E*) Comparisons of toughness for polyurethane–PDMS films from *A* and *B*. (*F*) Comparisons of Young's modulus and toughness for polyurethane–PDMS films from (*C*). The error bars represent the SD of the measured values (n = 3).

(Fig. 3*F*). At a low nanofiber density, the decrease of the ratio between PDMS and nanofiber leads to thinner polyurethane–PDMS films with a stronger reinforcing effect, namely, with higher Young's modulus and toughness. Therefore, at a low nanofiber density, Young's modulus and toughness are inversely proportional to the thickness (*SI Appendix*, Fig. S11).

Adhesion Performance of Polyurethane–PDMS Nanofilms. Based on the thinness structure and adhesive property of PDMS (43), the nanofilm possesses high-performance self-adhesiveness. An intuitive demonstration of the self-adhesiveness is shown in Movie S3 and *SI Appendix*, Fig. S12*A*; the nanofilm behaves like a "sticky" glue while attaching to and peeling off from the human skin. The attached nanofilm can also move freely along with natural skin motions, such as straining and compressing (*SI Appendix*, Fig. S12*B*). The good dynamic adhesion is attributed to the capability of the nanofilm to stretch over large distances in all directions. However, ultrathin PDMS film exhibits obvious wrinkles after attachment to the skin (*SI Appendix*, Fig. S13). Nevertheless, the reported sub-300 nm Parylene/Au electrodes exhibit good self-adhesive properties (44); 200-nm-thick Parylene film can only be stretched to a less than 8% strain (*SI Appendix*, Fig. S14).

The adhesion performance of a polymeric film can be influenced by features such as surface chemistry (34), roughness (45, 46), and thickness (47). Dynamic adhesion is also influenced by Young's modulus of the film. We thus quantitatively studied the adhesion performance of the free-standing polyurethane–PDMS films via a tack separation test (34). The experimental setup and calculation method are described in Fig. 4*A* and *SI Appendix*, Fig. S15. The adhesion force was recorded by a high-precision tensile tester; the holder was gradually lifted at 10 mm/min until the suspended nanofilm was completely separated from the substrate. The adhesion energy per unit area (E) was characterized by the integrated area of adhesion force stroke curve; that is, $E = \int_0^X y dL$. Here, X, y, and L are separation stroke, adhesion force, and stroke, respectively.

In general, thinner polyurethane–PDMS nanofilms have larger adhesion energy as well as separation stroke (34). For instance, using nanofibers with a density of 0.36 mg/cm^2, the adhesion energy of 0.095-, 0.213-, and 1.653-μm-thick polyurethane–PDMS films decrease from 159.3 ± 2.4 to 78.8 ± 2.4 μJ/cm^2 (Fig. 4*B* and *SI Appendix*, Fig. S16*A*). Similarly, the separation strokes of 0.095-, 0.213-, and 1.653 μm-thick polyurethane–PDMS films gradually decline from 10.93 ± 0.15 to 6.23 ± 0.01 mm. In contrast, when the nanofiber density increases to 3.60 mg/cm^2, the influence of thickness on adhesion performance is reversed; that is, thicker polyurethane–PDMS films have larger separation stroke, adhesion energy, and separation force (Fig. 4*C* and *SI Appendix*, Fig. S16*B*). In specific, the adhesion energy of 0.461-, 1.239-, and 1.925-μm-thick polyurethane–PDMS films is 14.4 ± 1.1, 26.6 ± 0.9, and 62.1 ± 1.2 μJ/cm^2, respectively. The corresponding separation force escalates from 11.1 ± 0.3 to 25.3 ± 0.7 mN (*SI Appendix*, Fig. S17), and the separation stroke increases from 2.30 ± 0.04 to 4.06 ± 0.03 mm.

We further examined the adhesion performances of polyurethane–PDMS films with similar thicknesses (0.213 to 0.255 μm). They were fabricated with different nanofiber densities (0.36, 1.08, and 2.16 mg/cm^2) using different PDMS solutions. From the dynamic adhesion curves shown in Fig. 4*D*, it is unambiguous that higher nanofiber densities lead to smaller adhesion energy, separation stroke, and separation force. Particularly, in the case of 0.36 mg/cm^2, the initial values of adhesion energy, separation stroke, and separation force are 159.3 ± 2.4 μJ/cm^2, 8.98 ± 0.08 mm, and 28.9 ± 1.2 mN, respectively. When the nanofiber density is 2.16 mg/cm^2, these values decrease to 65.4 ± 4.3 μJ/cm^2, 5.28 ± 0.04 mm, and 22.1 ± 1.2 mN, respectively (Fig. 4*D* and *SI Appendix*, Fig. S17). Fig. 4*E* concludes the relationship between area adhesion energy, thickness, and nanofiber density, in which better adhesion performance can be achieved by thinner films with lower nanofiber densities. It is because 1) thinner films have more contact area with skin, enabling better adhesion; 2) films with smaller Young's modulus have larger separation stroke due to their softness; and 3) at a constant fiber density, the Young's modulus of the films is inversely proportional to the thickness.

To further evaluate the adhesion performance of nanofilms, ultrathin PDMS films (~720 nm thick) were prepared for comparison. Movie S4 demonstrates the detaching process of the nanofilm from an artificial skin surface, indicating its superior robustness and elasticity. The results show that the nanofilm exhibits a maximum separation force of 25.5 ± 0.8 mN and a separation stroke of up to 10.9 ± 0.2 mm. These values are 3.8 and 5 times larger than those of pure PDMS film, respectively (Fig. 4*F* and *SI Appendix*, Fig. S18*A*). The adhesion energy of the nanofilm was calculated to be 159.3 ± 2.4 μJ/cm^2 (Fig. 4*G*), outperforming that of 560-nm-thick polydopamine-modified PDMS film (50.7 μJ/cm^2) (34). The results prove that the nanofilm has outstanding self-adhesiveness, even with no surface modification for additional chemical bonding. It is because that the van der Waals forces exist over a larger contact area at the interface between nanofilm and the target surface (48). Particularly, good adhesion performance was maintained during 1,100 attaching and detaching adhesion cycles (Fig. 4*H* and *SI Appendix*, Fig. S18*B*).

The thinness and softness of the nanofilms enable unprecedented adaption to a substrate of capricious shape and roughness (49). We further investigated the adhesion properties of the nanofilms to other surfaces, such as metal, Parylene (hydrophobic), glass (hydrophilic), and biological tissue from swine liver (*SI Appendix*, Fig. S19). Parylene and glass substrates have a maximum adhesion force of over 16 mN, and metal substrates demonstrate the lowest separation stroke of ~6.5 mm. Parylene substrates show the highest adhesion energy of 78.4 ± 11.3 μJ/cm^2, followed by glass, metal, and biological tissue, with adhesion energies of 76.7 ± 4.4, 60.7 ± 5.1, and 55.7 ± 2.2 μJ/cm^2, respectively. It is concluded that the good adherence of the nanofilm is universal to various kinds of surfaces.

Free-Standing Nanofilm Dry Electrode for Long-Term ECG Monitoring. To be applicable as a long-term ECG dry electrode, the device should have high gas permeability, robustness, water resistance, strain insensitivity, skin compliance, and low skin impedance. It should also be comfortable to wear and capable of surviving motions and liquid environment during normal living behaviors. In this regard, we examined the feasibility of the developed nanofilms as elastomeric substrates for long-term dry electrodes. To achieve conductivity, 70-nm-thick Au was deposited onto the nanofilm. The resultant nanofilm electrode has an ultralight weight of 0.14 mg/cm^2. The shiny golden appearance of the Au-coated side of the nanofilm electrode is shown in *SI Appendix*, Fig. S20*A*. The back side of the nanofilm electrode is black, owing to the microscopic morphology of the surface of the polyurethane–PDMS nanofilm (50, 51) (*SI Appendix*, Fig. S20*B*). Both the Au side–attached nanofilm and the polyurethane–PDMS side–attached nanofilm electrodes exhibited high compliance with the human skin (*SI Appendix*, Fig. S20 *C–E*). After laminating nanofilm onto artificial skins, both the nanofilm side and Au side exhibit high adhesion energy (*SI Appendix*, Fig. S21). Nanofilm electrodes could also be patterned (with a resolution of 400 μm) and move freely with natural skin motions after attachment (*SI Appendix*, Fig. S22). A free-standing nanofilm electrode could be stretched to ~34% strain (Fig. 5*A*). Specifically, the relative change in resistance ($\Delta R/R_0$) was only 1.06 at 30% strain. Electromechanical durability was demonstrated by 1,000 cycles of stretching and releasing at 10, 15, and 20% strain,

ENGINEERING

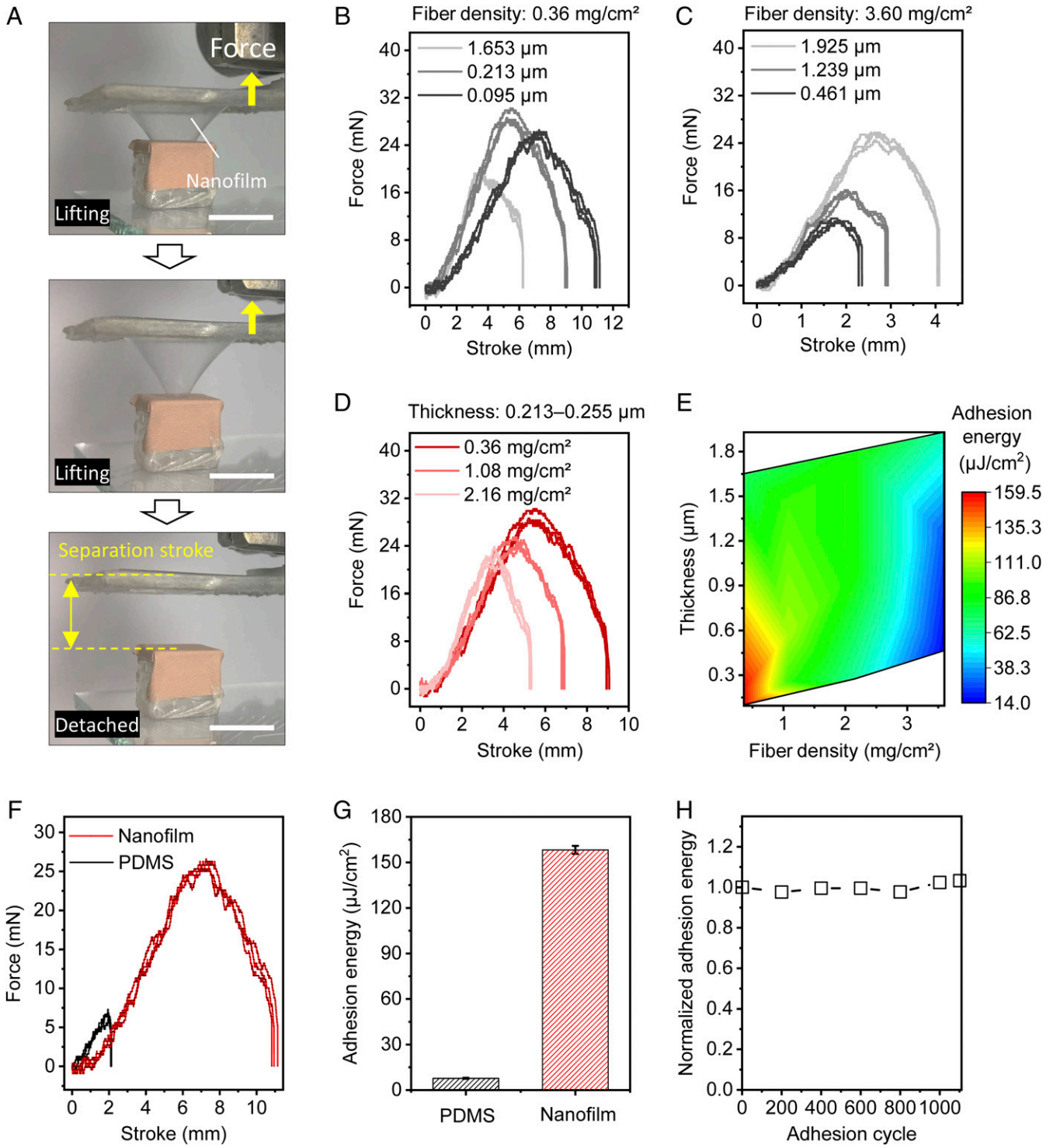

Fig. 4. Adhesion performance of free-standing polyurethane–PDMS films with different nanofiber densities and film thicknesses. Adhesion substrate: artificial skins. (*A*) Photographs showing the detaching process of the nanofilm from an artificial skin during a tack separation experiment. (Scale bar, 10 mm.) (*B*) Force stroke curves of different polyurethane–PDMS films (0.095, 0.213, and 1.653 μm thick). Fiber density: 0.36 mg/cm^2. (*C*) Force stroke curves of different polyurethane–PDMS films (0.461, 1.239, and 1.925 μm thick). Fiber density: 3.60 mg/cm^2. (*D*) Force stroke curves of polyurethane–PDMS films of similar thicknesses (0.213 to 0.255 μm) from different polyurethane nanofibers. Fiber densities: 0.36, 1.08, and 2.16 mg/cm^2. (*E*) Mapping of the adhesion energy distribution of polyurethane–PDMS films as a function of thickness and the density of polyurethane nanofibers. (*F–H*). Adhesion performance of 95-nm-thick free-standing polyurethane–PDMS nanofilms. (*F*) Force stroke curves of the nanofilms and ~720-nm-thick pure PDMS films on artificial skins. (*G*) Comparisons of adhesion energy and separation stroke for the nanofilms and pure PDMS films on artificial skins. (*H*) Normalized adhesion energy of the nanofilms during 1,100 attaching/detaching adhesion cycles. Error bars represent the SD of the measured values (n = 3).

respectively (Fig. 5*B*). The durability performance is originated to the reversible wrinkle propagations during stretching and releasing processes (*SI Appendix*, Fig. S23).

To investigate the gas permeability of nanofilm electrodes, we carried out a water vapor transmission experiment. Both the nanofilm and nanofilm electrode demonstrated similar water transmission rates to those of an open bottle (*SI Appendix*, Fig. S24*A*). It is attributed to the gas permeability of thin PDMS films (52) and the nanovoids in the Au layer. However, ∼10-μm-thick PDMS film exhibited a smaller transmission rate; for ∼1.2-mm-thick PDMS, over 99% of water remained in the bottle. Contact angle measurements revealed that the nanofilm electrode exhibited hydrophobic behavior when fixed on a flat substrate, which was consistent with the behavior of the 1-mm-thick bulk PDMS film (*SI Appendix*, Fig. S24*B*). After adhering to the human skin, the nanofilm electrode exhibited excellent hydrophobic characteristics (Movie S5). Additionally, the resistance of the nanofilm electrode remained almost the same when immersed in vigorously stirring water for 40 h under a stirring rate of 850 rpm (*SI Appendix*, Fig. S24*C* and Movie S6).

For long-term ECG measurement, a pair of nanofilm electrodes was placed on the left inner wrist and right inner ankle of the subject for 1-wk continuous wearing (*SI Appendix*, Fig. S25*A*). With respect to the connection, adhesive and breathable 3M Tegaderm films were coated with Au and adhered to the human skin before electrode attachment (*SI Appendix*, Fig. S25*B*). Au/PDMS electrodes, referred to as PDMS electrodes, were used for comparison. After attachment, both nanofilm and PDMS electrodes exhibited comparable ECG signals with similar signal-to-noise ratios (SNRs) (Fig. 5 *C*–*E*). The nanofilm electrode was demonstrated to be robust for continuous wearing against normal living behaviors such as working and bathing for 1 wk (*SI Appendix*, Fig. S25*C*). The average SNR of 1-wk measurement was 34.1 dB, which was close to that of commercial gel electrodes (∼34.6 dB) (Fig. 5*E* and *SI Appendix*, Fig. S26 *A* and *B*). Fig. 5*F* shows that the contact skin impedance of the nanofilm electrodes was comparable to that of commercial gel electrodes even after showers, though gel ECG electrodes experienced severe delamination and leakage after shower (*SI Appendix*, Fig. S26 *C* and *D*). ECG signals were also successfully recorded under motion using nanofilm electrodes (*SI Appendix*, Fig. S26*E*). However, PDMS electrodes started to fracture after only 1.5 h wearing, leading to a reduced SNR of 18.8 dB (Fig. 5 *D* and *E*). They lost the functionality after 4 h wearing because of the severe mechanical damage caused by the inferior robustness (*SI Appendix*, Fig. S27).

Discussion

Compared to our previous work (8, 18) in which ultrasoft nanomesh sensors were attached onto the human skin using dissolved thin PVA films as an adhesive layer, the present polyurethane–PDMS nanofilm electrodes can self-adhere to the human skin and retain its functionality over 1 wk. The remarkable gas permeability, self-adhesiveness, and mechanical robustness are originated to its thinness and reinforcement structure. One promising advantage of the nanofilm dry electrodes is simultaneously having gas permeability, self-adhesiveness, and robustness. These features are significant in prolonged health monitoring for early disease diagnosis. The reported method is effective, universal, and scalable to fabricate robust, free-standing polymeric nanofilms by dip-coating electrospun nanofibers with a film-forming polymer solution. We envisage that the nanofilm systems in this work open opportunities for advanced skin/implantable devices for next-generation ambulatory monitoring systems.

Materials and Methods

Material Preparation. N, *N*-dimethylformamide (DMF), methyl ethyl ketone (MEK), and n-hexane were purchased from Wako Chemical Industries. PVA (EG-22P) was from Nippon Synthetic Chemical Industries. Artificial skin was purchased from Beaulax (BIOSKIN plate). A pristine polyurethane solution (Rezamin M-8115LP, 30 wt%) was provided by Dainichiseika. The electrospun polyurethane solution (13 wt%) was prepared by diluting it with a mixture of DMF and MEK (wt/wt = 7:3). A Teflon (AF1600, Dupont) solution (3 wt%) was prepared by dissolving it in a solvent (FC-43, 3M) and stirring for 6 h at 70 °C. Porous alumina membranes (Anodisc, pore size: 0.2 μm, diameter: 25 mm, thickness: 60 μm) were purchased from Whatman International. The PDMS precursor was prepared by mixing the Sylgard 184 silicone elastomer base and curing agent at a weight ratio of 10:1. The Ecoflex (00-30, Smooth-ON) precursor was prepared by mixing parts A and B at a weight ratio of 1:1. Commercial gel electrodes (Vitrode F-150SL) were purchased from Nihon Kohden. All chemicals were used as received unless otherwise indicated.

Thin Pure PDMS Film. The fabrication process is shown schematically in *SI Appendix*, Fig. S3. To produce a pristine PDMS film, PVA was utilized as a temporary substrate. Before spin coating the PVA layer using 10 wt% aqueous solution, a sacrificial layer of Teflon was spin coated onto a clean glass to achieve easy detachment of the PVA from the glass. Then, the diluted PDMS/hexane (6.3 wt%) solution was spin coated onto the PVA layer. After the PDMS film was fully cured, the PVA/PDMS was peeled off from the glass and transferred to a polyimide window with desired dimensions. A free-standing PDMS thin film was obtained by dissolving the PVA in water. We could achieve PDMS thin films with different thicknesses by varying the spin-coating rate.

Fabrication of Free-Standing Anofilms Using Electrospun Nanofibers. The fabrication process of polyurethane nanofibers has been reported previously (18). The parameters for electrospinning (NANON-03, Mecc Corp.) were as follows: a metallic needle with a diameter of 27 G, a voltage of 25 kV, a flow rate of 1.0 mL/h, and a distance of 12.5 cm between the needle tip and the grounded collector. A rotating drum (diameter: 20 cm, length: 20 cm) was covered with silicone-coated paper to collect polyurethane nanofiber sheets. In this study, polyurethane nanofiber densities of 0.36, 1.08, 2.16, and 3.60 mg/cm^2 were obtained. The polyurethane nanofiber sheet was then transferred to polyimide or poly(ethylene 2,6-naphthalate (PEN) windows with desired dimensions. The diluted PDMS solution was prepared by mixing the PDMS precursor with hexane at different concentrations (2.27, 2.94, 4.17, 5.26, 7.14, and 16.7 wt %). Finally, the polyurethane nanofiber was dip coated using diluted PDMS solution. The resultant polyurethane–PDMS films were cured fully at 80 °C for 3 h in an oven to achieve the polyurethane–PDMS nanofilms. Note that the dip-coating speed and soaking time were maintained at ∼60 mm/s and 2 s, respectively. To deposit gold, the suspended nanofilms were cured on a hot plate at 120 °C for 5 h.

Using the same technique, polyurethane–Ecoflex and polyurethane–PVA nanofilms were fabricated by dip coating the polyurethane nanofiber sheets (density: 2.16 mg/cm^2) into an Ecoflex prepolymer hexane solution (4.8 wt%) and a PVA aqueous solution (1.25 wt%), respectively. A 10 wt% PVA aqueous solution was used to produce the PVA nanofiber sheet (density: 2.16 mg/cm^2) (*SI Appendix*, Fig. S7). PVA–PDMS and PVA–polyurethane nanofilms were prepared by dip coating the PVA nanofiber sheets into PDMS hexane solution (7.14 wt%) and polyurethane solution (3.12 wt%), respectively. All films were cured at 80 °C for 3 h in an oven.

Optical microscopy images were recorded using a color 3D laser scanning microscope (VK-9710, Keyence). SEM imaging was performed using FE-SEM (S4800, Hitachi High Technologies). Metal deposition was performed using a thermal evaporator (EX-200, ULVAC).

Tensile Stress Test. All samples were transferred to a polyimide film with a window of 10 × 7 mm^2. Next, the samples were fixed vertically on the clamps of a high-precision tensile tester (AG-X, Shimadzu), which was separated from the polyimide window on the left and right borders using a sharp scalpel. The polyimide window was then carefully excised on the two sides before the measurement of tensile stress using the tensile tester.

Tack Separation Test. A 3D printed holder with a window of size 2 × 2 cm^2 was used to support the polyimide windows. All samples were transferred to polyimide windows (1.8 × 1.8 cm^2) and then fixed onto the holder. The initial adhesion area was 1 × 1 cm^2 between the suspended films and the surface of the target substrate (1 × 1 cm^2). The adhesion force was recorded using a high-precision tensile tester (AG-X, Shimadzu) when the holder was gradually lifted at 10 mm/min until complete separation from the substrate. The adhesion energy was calculated from the curve of the adhesion force versus stroke as described in *SI Appendix*, Fig. S15.

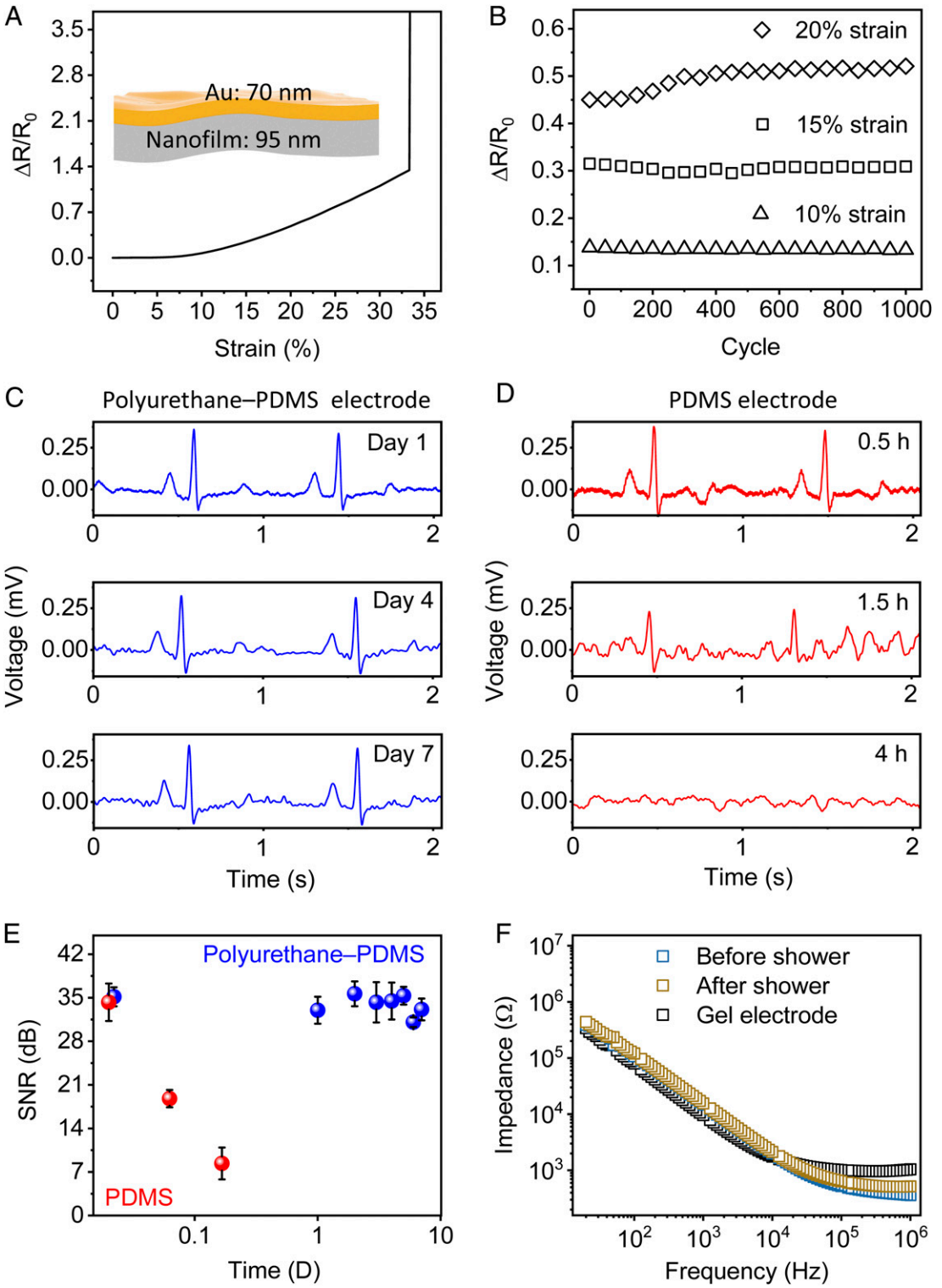

Fig. 5. Free-standing polyurethane–PDMS nanofilm electrodes and their application as long-term ECG dry electrodes. (*A*) Stretchability of the free-standing nanofilm electrode. (*Inset*) Structure of nanofilm electrode. (*B*) Cyclic test of the nanofilm electrode at 10, 15, and 20% strain. (*C*) ECG measurement of the nanofilm electrodes on day 1, 4, and 7, respectively. (*D*) ECG measurement of pure PDMS electrodes after attachment for 0.5, 1.5, and 4 h, respectively. (*E*) SNR of ECG measurements of the nanofilm and pure PDMS electrodes. (*F*) Comparison of skin contact impedance between commercial gel electrodes, nanofilm electrodes before shower, and nanofilm electrodes after shower. The error bars represent the SD of the measured values ($n = 3$).

Contact Angle Measurement. Contact angle measurements were conducted on pure bulk PDMS films (1 mm thick) and nanofilm electrodes. Nanofilm electrodes were fixed on glass slides with nanofilm sides exposed. Images of water droplets (0.6 μL) on the solid surfaces were automatically captured. The contact angles were automatically calculated by a machine (KYOWA DM-CE1 Contact Angle Meter).

Stretchability Test. The two ends of the free-standing nanofilm electrodes were fixed to a motorized moving stage (Thorlabs Model LTS150/M). Then, uniform stretching/releasing cycles were applied by a computer-based user interface (Thorlabs APT user), while the resistance was recorded using a digital multimeter (34410A, Keysight).

Water Vapor Transmission Test. The water vapor permeability was investigated by measuring the weight of a water-containing glass bottle. The bottle openings were sealed using different samples. Water (2.0 g) was placed in each bottle. The measurements were carried out while the samples were stored undisturbed in a thermostatic chamber at 21.5 °C and 11% humidity.

On-Skin Long-Term Monitoring. The detailed setup for long-term ECG monitoring is shown in *SI Appendix*, Fig. S25. Electrode size: 1.5×2.0 cm^2. Au was directly deposited onto the 95-nm-thick nanofilms without any surface treatment. The prepared nanofilm electrodes were laminated on the left inner wrist and right inner ankle of the subject, and a commercial gel electrode was attached to the left inner ankle as the reference electrode. The reference electrode was peeled off after each measurement. For external connections, thin breathable medical tape (3M Tegaderm) was first deposited by the 100-nm-thick Au layer. Then Au/Tegaderm adhered to the skin with the Au side exposed. Nanofilm electrodes were laminated on the skin with one end covering the exposed Au area of Au/Tegaderm. Alligator clips were connected to the end of the Au/Tegaderm film for the ECG measurements. The subject wore the nanofilm electrodes for 1 wk while performing daily life activities such as working and bathing. Daily showers were taken at a temperature of 37 °C, a duration of 12 to 15 min, and a water flow rate of ∼4.5 L/min. Skin contact impedance were measured using a precision LCR meter (E4980AL, Keysight). The ECG measurements were recorded daily using a Neuropack X1 (Nihon Kohden MEB-2300). In a control experiment, ∼720-nm-thick pure PDMS films were treated by mild ultraviolet ozone exposure (1 min) and subsequently coated with a 5-nm-thick chromium layer and a 70-nm-thick Au layer. ECG measurements were taken after 0.5, 1.5, and 4 h wearing. All ECG data acquired from the sedentary state were processed by a band-pass filter of 0.5 to100 Hz and a 50 Hz notch filter. ECG data acquired under motions were processed using a band-pass filter of 3 to 100 Hz and a 50 Hz notch filter. The ratio of the peak-to-peak voltage by the SD of the noise voltage was used to calculate the SNR.

Experiments on Human Subjects. The study protocol was thoroughly reviewed and approved by the ethical committee of The University of Tokyo (approval no. KE19-32), and informed consent was obtained from all participants for all experiments.

Data Availability. All study data are included in the article and/or *SI Appendix*.

ACKNOWLEDGMENTS. This work was financially supported by the Japan Science and Technology ACCEL (Grant No. JPMJMI17F1). We thank Dr. Chihiro Okutani and Akihito Miyamoto (The University of Tokyo) for helpful technical advice and scientific discussions.

1. D. H. Kim *et al.*, Epidermal electronics. *Science* **333**, 838–843 (2011).
2. Y. Kim *et al.*, A bioinspired flexible organic artificial afferent nerve. *Science* **360**, 998–1003 (2018).
3. T. Someya, Z. Bao, G. G. Malliaras, The rise of plastic bioelectronics. *Nature* **540**, 379–385 (2016).
4. A. K. Oktavius *et al.*, Fully-conformable porous polyethylene nanofilm sweat sensor for sports fatigue. *IEEE Sens. J.* **21**, 8861–8867 (2021).
5. K. Yamagishi, S. Takeoka, T. Fujie, Printed nanofilms mechanically conforming to living bodies. *Biomater. Sci.* **7**, 520–531 (2019).
6. T. Someya, M. Amagai, Toward a new generation of smart skins. *Nat. Biotechnol.* **37**, 382–388 (2019).
7. D. H. Kim *et al.*, Dissolvable films of silk fibroin for ultrathin conformal bio-integrated electronics. *Nat. Mater.* **9**, 511–517 (2010).
8. S. Lee *et al.*, Nanomesh pressure sensor for monitoring finger manipulation without sensory interference. *Science* **370**, 966–970 (2020).
9. S. M. Lee *et al.*, Self-adhesive epidermal carbon nanotube electronics for tether-free long-term continuous recording of biosignals. *Sci. Rep.* **4**, 6074 (2014).
10. A. Searle, L. Kirkup, A direct comparison of wet, dry and insulating bioelectric recording electrodes. *Physiol. Meas.* **21**, 271–283 (2000).
11. H. Wu *et al.*, Materials, devices, and systems of on-skin electrodes for electrophysiological monitoring and human–machine interfaces. *Adv. Sci. (Weinh.)* **8**, 2001938 (2020).
12. H. C. Jung *et al.*, CNT/PDMS composite flexible dry electrodes for long-term ECG monitoring. *IEEE Trans. Biomed. Eng.* **59**, 1472–1479 (2012).
13. L. Zhang *et al.*, Fully organic compliant dry electrodes self-adhesive to skin for long-term motion-robust epidermal biopotential monitoring. *Nat. Commun.* **11**, 4683 (2020).
14. J. Y. Baek, J. H. An, J. M. Choi, K. S. Park, S. H. Lee, Flexible polymeric dry electrodes for the long-term monitoring of ECG. *Sens. Actuators A Phys.* **143**, 423–429 (2008).
15. W. Dong, X. Cheng, T. Xiong, X. Wang, Stretchable bio-potential electrode with self-similar serpentine structure for continuous, long-term, stable ECG recordings. *Biomed. Microdevices* **21**, 6 (2019).
16. S. Kabiri Ameri *et al.*, Graphene electronic tattoo sensors. *ACS Nano* **11**, 7634–7641 (2017).
17. Y. Wang, T. Yokota, T. Someya, Electrospun nanofiber-based soft electronics. *NPG Asia Mater.* **13**, 22 (2021).
18. Y. Wang *et al.*, A durable nanomesh on-skin strain gauge for natural skin motion monitoring with minimum mechanical constraints. *Sci. Adv.* **6**, eabb7043 (2020).
19. X. Yang *et al.*, Ultrathin, stretchable, and breathable epidermal electronics based on a facile bubble blowing method. *Adv. Electron. Mater.* **6**, 2000306 (2020).
20. Z. Ma *et al.*, Permeable superelastic liquid-metal fibre mat enables biocompatible and monolithic stretchable electronics. *Nat. Mater.* **20**, 859–868 (2021).
21. A. Miyamoto *et al.*, Inflammation-free, gas-permeable, lightweight, stretchable on-skin electronics with nanomeshes. *Nat. Nanotechnol.* **12**, 907–913 (2017).
22. Y. Fang *et al.*, Solution-processed submicron free-standing, conformal, transparent, breathable epidermal electrodes. *ACS Appl. Mater. Interfaces* **12**, 23689–23696 (2020).
23. L. Liu *et al.*, Nanofiber-reinforced silver nanowires network as a robust, ultrathin, and conformable epidermal electrode for ambulatory monitoring of physiological signals. *Small* **15**, e1900755 (2019).
24. H. Chae *et al.*, Laser-processed nature-inspired deformable structures for breathable and reusable electrophysiological sensors toward controllable home electronic appliances and psychophysiological stress monitoring. *ACS Appl. Mater. Interfaces* **11**, 28387–28396 (2019).
25. Y. J. Fan *et al.*, Highly robust, transparent, and breathable epidermal electrode. *ACS Nano* **12**, 9326–9332 (2018).
26. W. Zhou *et al.*,Gas-permeable, ultrathin, stretchable epidermal electronics with porous electrodes. *ACS Nano* **14**, 5798–5805 (2020).
27. Z. Jiang *et al.*, Highly stretchable metallic nanowire networks reinforced by the underlying randomly distributed elastic polymer nanofibers via interfacial adhesion improvement. *Adv. Mater.* **31**, e1903446 (2019).
28. E. Kang *et al.*, Large-scale, ultrapliable, and free-standing nanomembranes. *Adv. Mater.* **25**, 2167–2173 (2013).
29. A. Zucca *et al.*, Roll to roll processing of ultraconformable conducting polymer nanosheets. *J. Mater. Chem. C Mater.* **25**, 6539–6548 (2015).
30. J. A. Rogers, Wearable electronics: Nanomesh on-skin electronics. *Nat. Nanotechnol.* **12**, 839–840 (2017).
31. T. Fujie, Development of free-standing polymer nanosheets for advanced medical and health-care applications. *Polym. J.* **48**, 773–780 (2016).
32. M. F. Jimenez-Solomon, Q. Song, K. E. Jelfs, M. Munoz-Ibanez, A. G. Livingston, Polymer nanofilms with enhanced microporosity by interfacial polymerization. *Nat. Mater.* **15**, 760–767 (2016).
33. F. Greco *et al.*, Ultra-thin conductive free-standing PEDOT/PSS nanofilms. *Soft Matter* **7**, 10642–10650 (2011).
34. K. Yamagishi *et al.*, Tissue-adhesive wirelessly powered optoelectronic device for metronomic photodynamic cancer therapy. *Nat. Biomed. Eng.* **3**, 27–36 (2019).
35. A. Mersha, S. Fujikawa, Mechanical reinforcement of free-standing polymeric nanomembranes via aluminosilicate nanotube scaffolding. *ACS Appl. Polym. Mater.* **1**, 112–117 (2019).
36. N. Sato, A. Murata, T. Fujie, S. Takeoka, Stretchable, adhesive and ultra-conformable elastomer thin films. *Soft Matter* **12**, 9202–9209 (2016).
37. Y. Okamura, K. Kabata, M. Kinoshita, D. Saitoh, S. Takeoka, Free-standing biodegradable poly (lactic acid) nanosheet for sealing operations in surgery. *Adv. Mater.* **21**, 4388–4392 (2009).
38. S. Karan, Z. Jiang, A. G. Livingston, MEMBRANE FILTRATION. Sub-10 nm polyamide nanofilms with ultrafast solvent transport for molecular separation. *Science* **348**, 1347–1351 (2015).
39. M. C. Salcedo, I. B. Coral, G. V. Ochoa, Characterization of surface topography with abbott firestone curve. *Contemp. Eng. Sci.* **11**, 3397–3407 (2018).

40. G. D. Genesky, C. Cohen, Toughness and fracture energy of PDMS bimodal and trimodal networks with widely separated precursor molar masses. *Polymer (Guildf.)* **51**, 4152–4159 (2010).
41. S. Jiang *et al*., Electrospun nanofiber reinforced composites: A review. *Polym. Chem.* **9**, 2685–2720 (2018).
42. Y. Shen *et al*., Electropunk nanofiber reinforced all-organic PVDF/PI tough composites and their dielectric permittivity. *Mater. Lett.* **160**, 515–517 (2015).
43. E. Kroner, R. Maboudian, E. Arzt, Adhesion characteristics of PDMS surfaces during repeated pull-off force measurements. *Adv. Eng. Mater.* **12**, 398–404 (2010).
44. R. A. Nawrocki *et al*., Self-adhesive and ultra-conformable, sub-300 nm dry thin-film electrodes for surface monitoring of biopotentials. *Adv. Funct. Mater.* **28**, 1803279 (2018).
45. B. N. Persson, O. Albohr, U. Tartaglino, A. I. Volokitin, E. Tosatti, On the nature of surface roughness with application to contact mechanics, sealing, rubber friction and adhesion. *J. Phys. Condens. Matter* **17**, R1–R62 (2005).
46. S. Kim *et al*., Microstructured elastomeric surfaces with reversible adhesion and examples of their use in deterministic assembly by transfer printing. *Proc. Natl. Acad. Sci. U.S.A.* **107**, 17095–17100 (2010).
47. T. Fujie *et al*., Adhesive, flexible, and robust polysaccharide nanosheets integrated for tissue-defect repair. *Adv. Funct. Mater.* **19**, 2560–2568 (2009).
48. M. Kaltenbrunner *et al*., An ultra-lightweight design for imperceptible plastic electronics. *Nature* **499**, 458–463 (2013).
49. R. A. Nawrocki, N. Matsuhisa, T. Yokota, T. Someya, 300-nm imperceptible, ultraflexible, and biocompatible e-skin fit with tactile sensors and organic transistors. *Adv. Electron. Mater.* **2**, 1500452 (2016).
50. Y. Wang *et al*., Unconventional Janus properties of enokitake-like gold nanowire films. *ACS Nano* **12**, 8717–8722 (2018).
51. C. Ng, L. W. Yap, A. Roberts, W. Cheng, D. E. Gómez, Black gold: Broadband, high absorption of visible light for photochemical systems. *Adv. Funct. Mater.* **27**, 1604080 (2017).
52. A. Lamberti, S. Marasso, M. J. R. A. Cocuzza, PDMS membranes with tunable gas permeability for microfluidic applications. *RSC Adv.* **4**, 61415–61419 (2014).